DOI: 10.13009/EUCASS2025-214
11TH EUROPEAN CONFERENCE FOR AERONAUTICS AND SPACE SCIENCES (EUCASS)

Experimental Investigation of Fluid Impact on Landing Behaviour of Vertically Landing Vehicles

Caroline Krämer[*†] and Lars Witte*[*]*
** German Aerospace Center, Institute of Space Systems, Landing and Exploration Technologies*
Robert-Hooke Straße 7, 28359 Bremen, Germany
caroline.kraemer@dlr.de – lars.witte@dlr.de
[†] Corresponding Author

Abstract

As reusability is gaining importance in space flight, launch vehicles are under development, where non-neglectable amounts of liquid propellant interact with the vehicle in the moment of touchdown. This paper proposes the experimental investigation of fluid-vehicle interaction upon touchdown of vertically landing space vehicles. Here, the test setup and execution of a landing test campaign with a fully functional touchdown demonstrator, containing a liquid filled tank are presented. Test data are presented briefly and repeatable test conditions and thus, repeatable landing conditions are proven.

1. Introduction

As reusability gains importance in the space launch sector, several programs are dedicated worldwide to the development of reusable launch vehicles (RLV). One of the most challenging phases for a RLV is the landing phase, which includes the critical touchdown event, since an unsuccessful landing will cause the loss of the vehicle. Residual liquid propellant remaining in the tanks during touchdown exhibits a sloshing motion, when exited. For applications, such as the lunar starship, that have large height of centre of gravity H_{COG} to footpad diameter d_F ratios and carry unneglectable amount of liquid propellant during touchdown, the sloshing fluid can affect the vehicle's dynamics, interact with the vehicle structure and induce new load cases. Therefore, the investigation of fluid induced effects during touchdown is indispensable for the design of RLV.

While numerous studies have been dedicated to investigate the in-flight fluid impact with regards to the effects on space craft dynamics, flight stability and guidance, navigation, attitude and control systems [1-14], only few studies address the fluid impact during touchdown. K. Anii et al [15] and Y. Furuich [16] numerically and experimentally investigated the sloshing impact in spherical tanks on landing dynamics of small body landers under microgravity conditions. Roithmayr and Pei numerically investigate the sloshing impact on landing stability for landers under lunar gravity [17]. Their work addresses a two-dimensional multibody modelling approach, consisting of a rigid pendulum, representing the sloshing fluid, attached to a rigid lander model. They offer first insights on how propellant sloshing affects the landing stability under varying landing conditions to provide preliminary design trends. Being intended for the early design phase, no details of landing gear articulation, energy absorption and elasticity are considered. Therefore, the impact of these parameters on the landing dynamics is being neglected and no options for the examination of fluid-structure interactions during touchdown are given. For the detailed RLV design the interaction of all vehicle parameters and their influence on the landing behaviour must be considered. Numerical parametric multibody studies offer a time and cost-efficient way to study a broad parameter spectrum and multiple vehicle configurations. However, such studies rely on experimental data for validation. Therefore, the experimental investigation of the landing behaviour of a vertically landing vehicle under sloshing impact is proposed, where the main test objectives are to provide experimental data

1) to prove repeatable landing behaviour under fluid impact and thus prove that constant landing conditions can be provided and results are comparable for further investigation,
2) for the investigation and characterization of the fluid sloshing impact on dynamical behaviour with regards to landing stability,

DOI: 10.13009/EUCASS2025-214

3) for the analysis of the fluid-structure interaction of the tank with regards to structural responses induced by the fluid

under varying landing conditions. The obtained data serve as validation basis for numerical models, with which parametric studies can be performed. This paper presents the test setup and execution of a landing test campaign with a fully functional touchdown demonstrator (TDD), containing a fluid filled tank. A detailed description of the TDD and the test facility are given in chapter 2. The test execution, including the test programme are presented in chapter 3. Test results are exemplarily presented in chapter 4, as a more detailed analysis is given in [18]. Chapter 5 concludes with a summary and conclusion.

2. Test setup

2.1. Touchdown demonstrator

As test object a touchdown demonstrator (TDD) (Figure 1) is used, that represents the kinematics and dynamics of a RLV, so the obtained data can directly be used for the validation of a numerical touchdown simulator. For this no subscale model of any specific vehicle is necessary. The TDD is based on an already existing lander engineering model (LEM) platform (Figure 1 (1)) [19]. The LEM is expanded by a lightweight aluminium profile support structure to accommodate a tank (Figure 1 (3)). As RLV tend to have a higher H_{COG}/D_F ratio than conventional planetary landers, the tank is to be positioned at the highest possible position as technically permitted. The maximum height of the TDD is limited by the working space of the test facility and results in approx. 3000 mm. Two reinforcement rings (Figure 1 (2)) are implemented to ensure torsional stiffness. At the top of the TDD a robot interface (Figure 1 (4)) is combined with a horizontal reinforcement structure, that prevents the vertical profiles from bending inwards when being lifted to the drop position. The maximum total mass of the TDD is 500 kg, corresponding to the maximal static load bearing capacity of the robot, which is used to lift the TDD to its drop position. To ensure a constant TDD mass throughout all test cases, with and without fluid, extra masses can be accommodated within the TDD's tip.

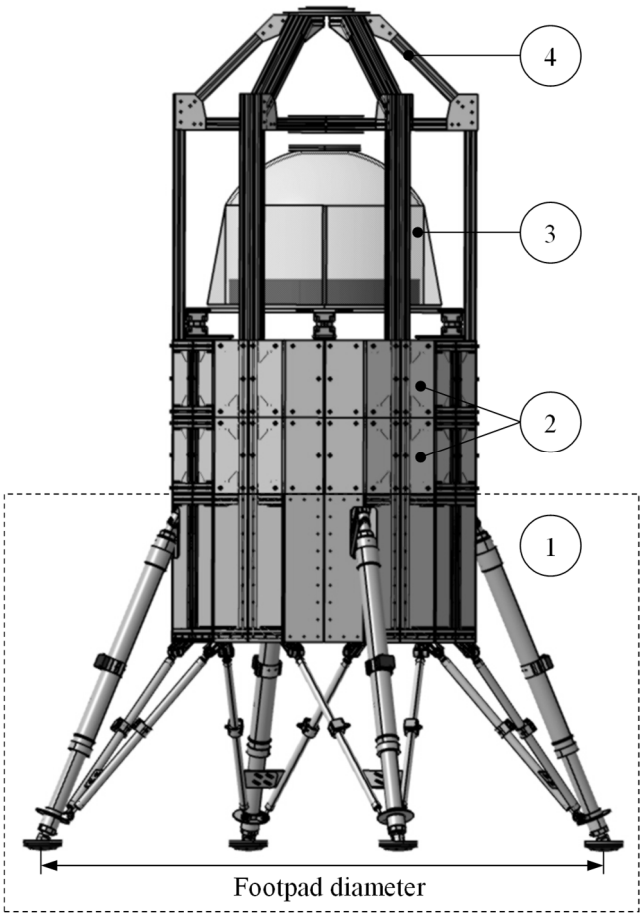

Figure 1: Touchdown Demonstrator

DOI: 10.13009/EUCASS2025-214

The LEM, depicted in Figure 2, is made up of a lander body and four landing legs. The lander body consists of lightweight aluminium profile frame, an aluminium baseplate (f) and aluminium cover sheets (e) to ensure torsional stiffness. The landing legs are used in an inverted tripod configuration, equivalent to state of the art RLV [20, 21]. Every leg consists of one aluminium primary telescopic strut (b), inluding an internal energy absorption mechanism, two aluminium secondary struts (a) and a fixed aluminium-rubber footpad. Cardan joints (d) serve as interfaces between the primary struts and the lander body (e). Interfaces (g) at the lander body baseplate (f) provide a connection for the secondary struts.

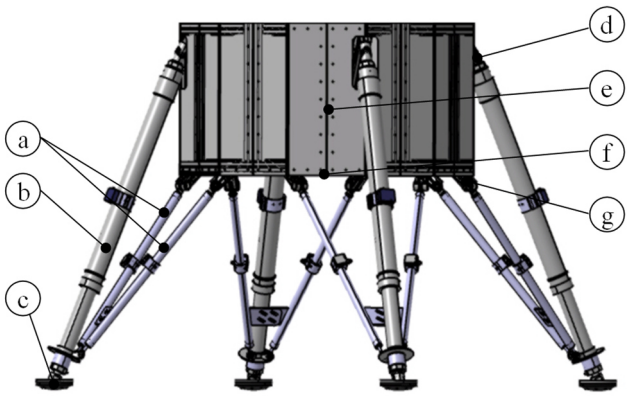

Figure 2: Lander Engineering Model used as TDD platform

Stiff footpads are used, where the angle between the footpad and the primary strut is fixed. This configuration corresponds to state of the art RLV footpads and poses mass advantages over a ball joint configuration. The footpad is depicted in Figure 3. The footpad-primary strut interface consists of two parts, one upper part, which is screwed onto the bottom part of the primary strut and an angled part to which the aluminium plate is mounted. Between these interface parts force sensors can be mounted to measure compressive and tensile forces within the leg. The aluminium plate serves as mounting point for the curved rubber piece, which provides a consistent contact surface between the footpad and the ground as the footpads slide outwards when the footpad diameter increases upon touchdown. Thin metal rings are used as spacers to ensure a correct alignment of the footpads, when screwed onto the primary strut.

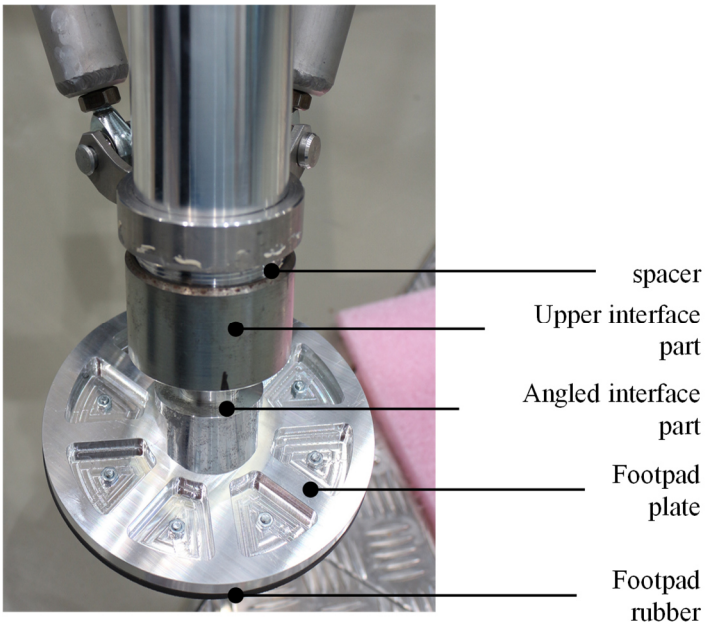

Figure 3: Footpad

Each primary strut contains two aluminium honeycomb cartridges as internal energy absorption mechanism, that are crushed upon touchdown. A retention mechanism prevents the telescopic primary strut from extending again after having been stowed due to impact, in case the TDD bounces or tilts upon touchdown. Both, the honeycomb

DOI: 10.13009/EUCASS2025-214

cartridges and the retention mechanism have to be exchanged or reset, respectively, during refurbishment after each test.

Leg 1 and adjacent leg 2, which correspond to the front and rear left leg respectively, are being equipped with sensors, as shown in Figure 4. Triaxial force sensors ($F_{FP,1}$ and $F_{FP,2}$) are placed between the footpad and the primary strut. The sensors are integrated such that the sensors' z-axes are aligned with the primary struts. Uniaxial force sensors ($F_{PS1,LB}$, $F_{PS2,LB}$, F_{SS11}, F_{SS12}, F_{SS21} and F_{SS22}) are placed at the top of the primary struts, right before the cardan lander body interface, and at top of the secondary struts, right before the lander body interfaces. The sensors' measurement axes are aligned with the primary strut axes and secondary struts axes, respectively. Laser range finders (LRF) are attached to the primary and secondary struts and measure the stroke along the struts' axes and underneath the lander body baseplate to measure the ground clearance. Leg 1 is additionally equipped with accelerometers, which are positioned on the footpad (Acc_{FP1}) as well as on all three interfaces to the lander body ($Acc_{PS1,LB}$, $Acc_{SS11,LB}$ and $Acc_{SS12,LB}$). The accelerometers measure the acceleration along the global vertical axis. On the baseplate inside the lander body a triaxial accelerometer (Acc_{LB}) and an inertial measurement unit (IMU) are positioned.

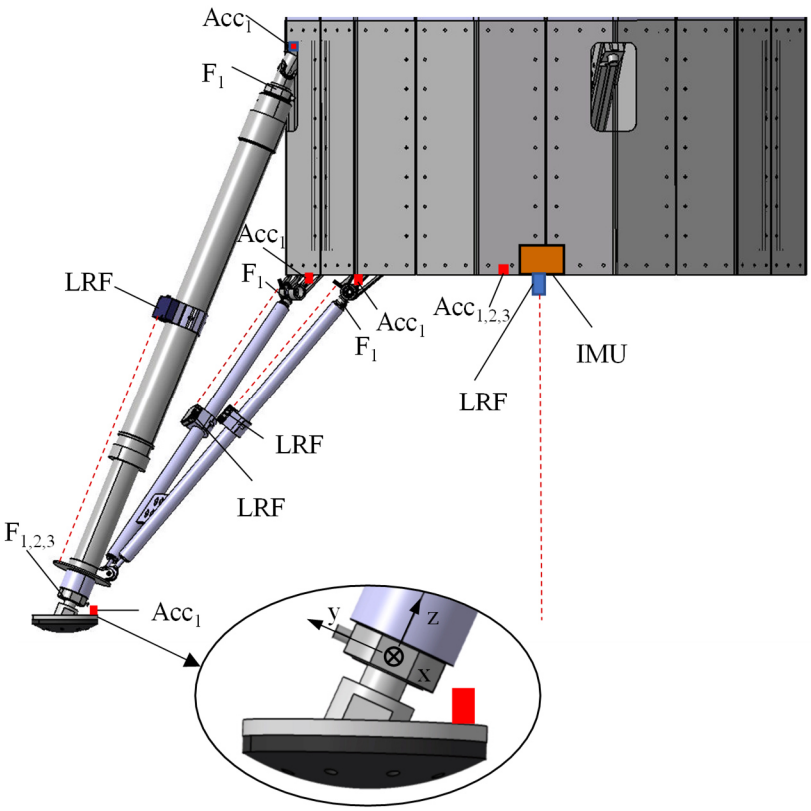

Figure 4: Sensor Locations Leg and Body

The tank (Figure 5) has a cylindrical shape with a dome shaped cap, including a detachable filling opening and is made of acrylic glass for visual detection of the fluid movement. De-mineralized water is chosen as test fluid, as its parameters are well known and it poses no handling risks. It is non-toxic and can be coloured for better visual detection. The tank base plate is made of aluminium and supported by four triaxial force sensors (F_{T1} – F_{T4}). Six uniaxial strain gauges and a triaxial accelerometer are attached to the bottom side of the base plate, as shown in Figure 5. Further, two accelerometers and four biaxial strain gauges are installed at the tank wall (Figure 5), at about 10 cm tank height, which is the height of the water edge for 50 l of water. In the middle of the bottom side of the baseplate a draining valve is installed, through which the tank can be emptied.

DOI: 10.13009/EUCASS2025-214

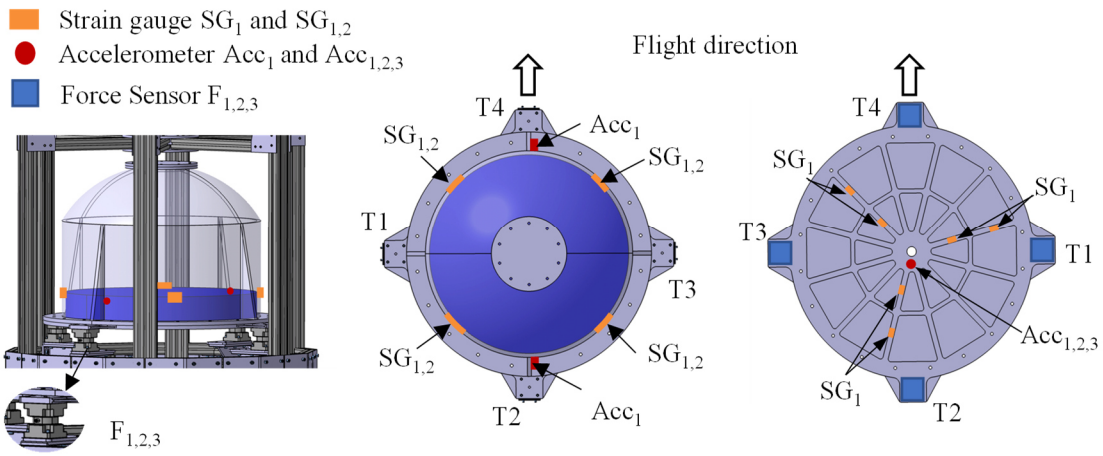

Figure 5: Sensor Locations Tank

2.2. Test Facility

The tests are performed in the Landing and Mobility Test Facility (LAMA) at the DLR-institute of space systems in Bremen [22], shown in Figure 6. The LAMA laboratory consists of a test cell, surrounded by a protective fence and a control and work space outside the fence. The test cell includes a landing area and is equipped with a 6-axis industrial robot system KR500 with an additional rail track system for horizontal movement (max. 1.5 m/s in both directions). As the robot follows a pre-programmed path, the test sequence can be completely automated and constant drop conditions and a precision landing can be ensured. At the release point the test object will have the pre-defined horizontal velocity. The release height has to be chosen with respect to the test object's size, so that the required vertical landing velocity is achieved by the free fall until ground contact. For this campaign the landing zone is equipped with concrete plates, placed on rubber mats to prevent sliding during touchdown. The concrete plates are chosen to ensure defined touchdown conditions in terms of stiffness and roughness.

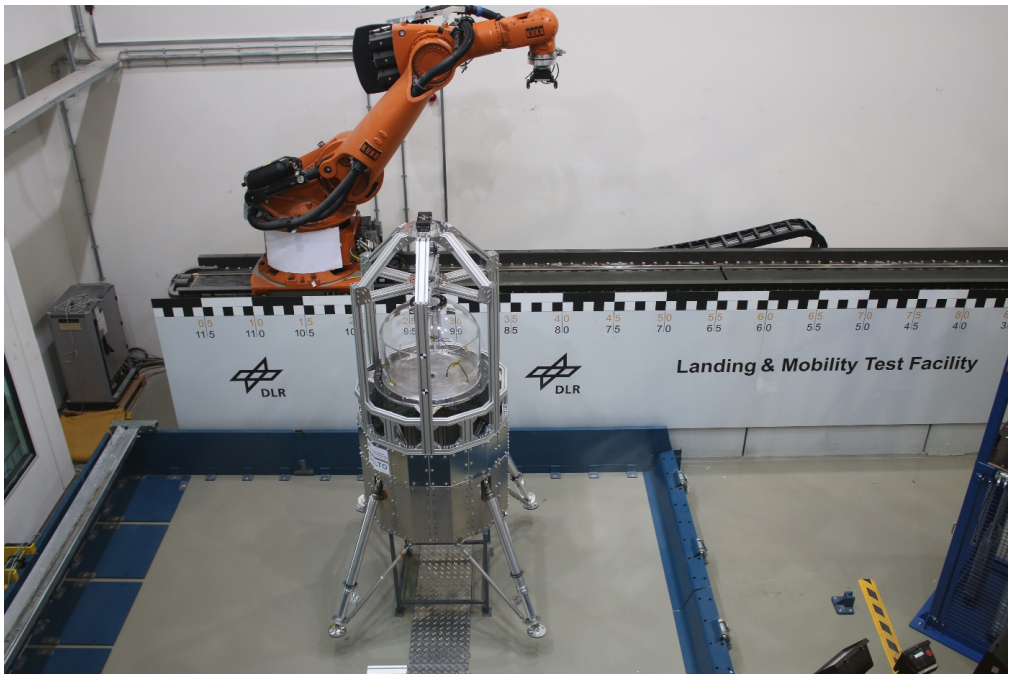

Figure 6: Landing and Mobility Test Facility at DLR Bremen

DOI: 10.13009/EUCASS2025-214

LAMA is equipped with an HBM QuantumX data acquisition system, which is used to record all sensor data at a 19.2 kHz sample rate. The IMU poses an autonomous system and acquires data at a sample rate of 50 Hz. In addition to the sensor data, a camera system is set up for visual documentation and motion tracking, as shown in Figure 7.
Two high speed cameras are used. Highspeed camera 1 (HS1) makes close up videos of the tank during touchdown, where special attention is needed. The HS2 camera is placed in a far perspective of the landing. Both high speed cameras are mounted on the LAMA fence. A HD reflex camera (canon) is positioned in front of the test setup, providing a front view.

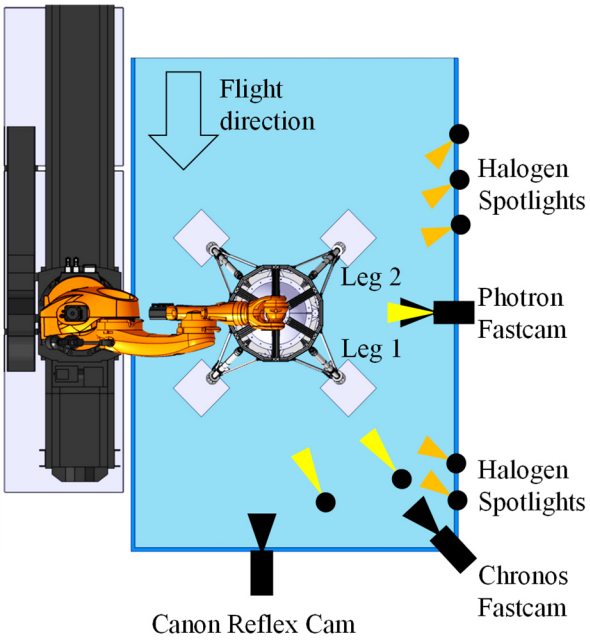

Figure 7: Camera Setup

3. Test execution

3.1. Test programme and configurations

All tests are conducted with a 2-2 configuration, at which the TDD has two leading and two trailing legs. This configuration is chosen to ensure a repeatable tilting axis, which is perpendicular to the horizontal landing velocity vector. The total TDD mass is kept constant throughout the test campaign at approx. 500 kg. The test parameters are driven by two rationale. On the one hand, it is aimed for high energy input, within the capability levels of the test facility, to generate significant responses from which the sloshing impact can be derived. On the other hand, the test parameters shall be of comparable magnitude of typical landing test parameters to ensure structural integrity. During all tests the TDD has the vertical landing velocity of 3.5 m/s, which is comparable to typical VTVL vehicle vertical landing velocities [23, 24]. To investigate the fluid impact on the landing behaviour of the TDD and on the structural responses, drop tests with three different fill levels are conducted:

- Fill level 1: 0 l of water
- Fill level 2: 50 l of water
- Fill level 3: 75 l of water

Fill level 1 serves as reference. At fill level 2 the fluid mass corresponds to 10 % of the total TDD mass, which corresponds to maximum residual fuel levels upon touchdown for scientific flight experiments. At fill level 3 approx. 40% of the tank are filled, which correlates with the fill level for which the highest sloshing impact is expected [25]. This fill level range corresponds to expected propellant masses for different VTVL vehicle applications during touchdown. This includes residual propellant mass for successful landing, propellant masses present in landing vehicles, which are supposed to take off and return from extra-terrestrial bodies or propellant masses required as ballistic masses for test flight conditions [26].
Depending on the fluid level, extra masses are added to the tip of the TDD to keep the total mass constant throughout the test campaign. The mass distribution is shown in Figure 8. The masses are mounted to the aluminum profiles and distributed symmetrically. For fill levels 2 and 3, where the mass distribution is not even among all six profiles, symmetry about the middle axis, perpendicular to the flight direction is ensured, so the tilting motion is not affected.

DOI: 10.13009/EUCASS2025-214

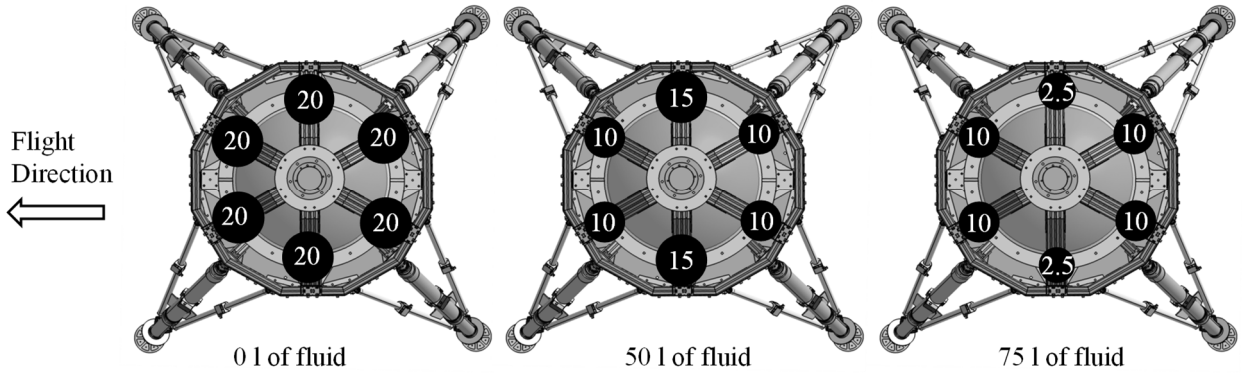

Figure 8: Mass distribution of extra masses in kg depending on the fill level

For each fill level different horizontal landing velocities are tested, as effects that affect the landing stability and landing dynamics only occur at horizontal landing velocities greater than 0 m/s:

- a) $v_H = 0$ m/s
- b) $v_H = 0.5$ m/s
- c) $v_H = 1$ m/s

Tests with $v_H = 0$ m/s serve as reference and are necessary to examine the structural responses at different fill levels and distinguish between structural responses due to the fluid impact and those due to dynamic effects. As the sloshing amplitude and thus the sloshing impact on the landing dynamics of the TDD are expected to grow with increasing horizontal landing velocity, two additional horizontal velocities are tested. For each fill level tests with $v_H = 0.5$ m/s are conducted. For the fill level extrema of 0 l and 75 l additional tests with $v_H = 1$ m/s are conducted. Both values lie within the capabilities of the test facility and are based on previous landing test campaigns and hence, are expected not to peril the structural integrity of the TDD but, nonetheless, induce measurable sloshing impacts.
This results in eight different test cases as listed in table 1. Two tests are conducted for each test case to prove non-chaotic and repeatable landing behaviour.

Table 1: Test Plan with Test Parameters

Case	Fill level [l]	Structural Mass [kg]	Extra masses [kg]	Total mass [kg]	V_V [m/s]	V_H [m/s]
1a	0	~375	120	~495	3.5	0
1b	0	~375	120	~495	3.5	0.5
1c	0	~375	120	~495	3.5	1
2a	50	~375	70	~495	3.5	0
2b	50	~375	70	~495	3.5	0.5
3a	75	~375	45	~495	3.5	0
3b	75	~375	45	~495	3.5	0.5
3c	75 l	~375	45	~495	3.5	1

3.2. Test sequence

Each test follows the same test sequence which is depicted in Figure 9. The TDD is attached to the robot, being at rest at its starting position (1), which varies with the desired horizontal landing velocity. Once receiving the start signal (1), which is triggered manually, the robots follows a predefined path until the gripper interface opens (2) and releases the TDD at the release position. The TDD performs a free fall (3), reaching its desired vertical landing velocity upon touchdown, followed by a tilting and bouncing motion (4) until all kinetic energy has ceased. Once at rest again (5), the TDD is refurbished (7), the retaining mechanisms at the primary struts are reset, all honeycomb cartridges are exchanged and potentially, configuration changes are performed.

DOI: 10.13009/EUCASS2025-214

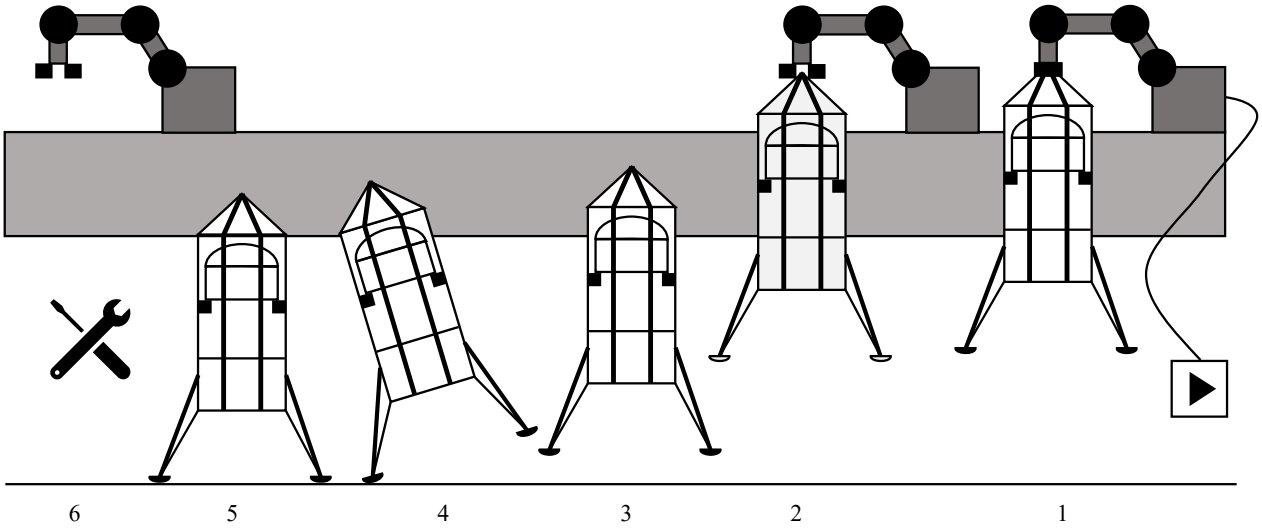

Figure 9: Schematic sketch of test sequence

4. Results

4.1. Repeatable landing conditions

Repeatable test conditions have to be provided to ensure repeatable landing conditions. Examination of the inertial robot data reveals equal force, acceleration and velocity curves for repetitions of the same test case are achieved. This is shown exemplarily for tests 3c.1 and 3c.2, which are the ones with highest fluid mass and horizontal landing velocity. The robot interface gripper forces in flight direction $F_{R,x}$ and in vertical direction $F_{R,z}$, the robot velocity in flight direction $v_{R,x}$ and acceleration in flight direction $a_{R,x}$ of tests 3c.1 and 3c.2 are shown in Figure 10. Time t = 0.0 s marks the release moment, when the interface gripper opens. It can be seen that for both test repetitions equal release conditions are achieved.

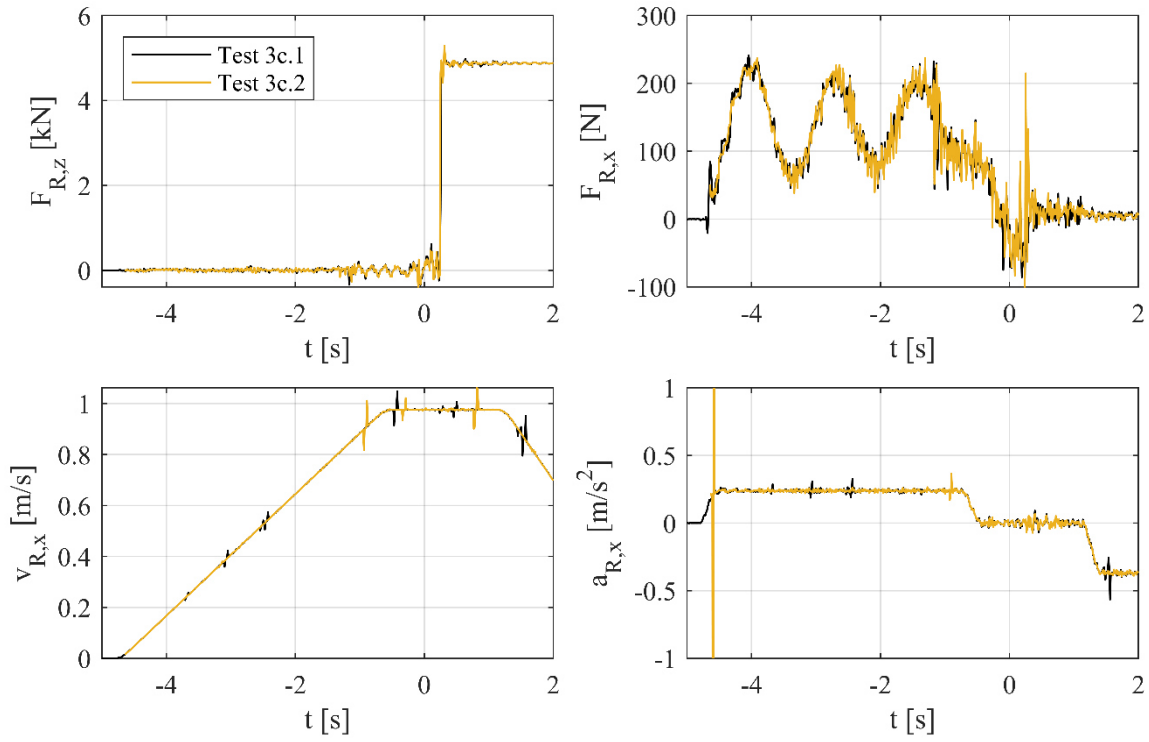

Figure 10: Robot interface forces and in vertical $F_{R,z}$ and flight direction $F_{R,x}$, robot velocities $v_{R,x}$ and accelerations $a_{R,x}$ for tests 3c.1 and 3c.2

DOI: 10.13009/EUCASS2025-214

Robot data of test cases 1c and 3c are compared to identify the possible relations between the robot movement and the fluid behaviour. As shown in Figure 11, no couplings between robot and fluid movement can be detected. The gripper interface force curves and the acceleration curves for both test cases are congruent. It is concluded that the oscillations seen in the gripper interface forces $F_{R,x}$ are due to slight TDD oscillations resulting from the start up accelerations and not due to sloshing fluid. This observation is confirmed by video material just before touchdown (t = 0 s), as exemplarily shown for test 3b.1 in Figure 12, where no significant fluid motion is detected.

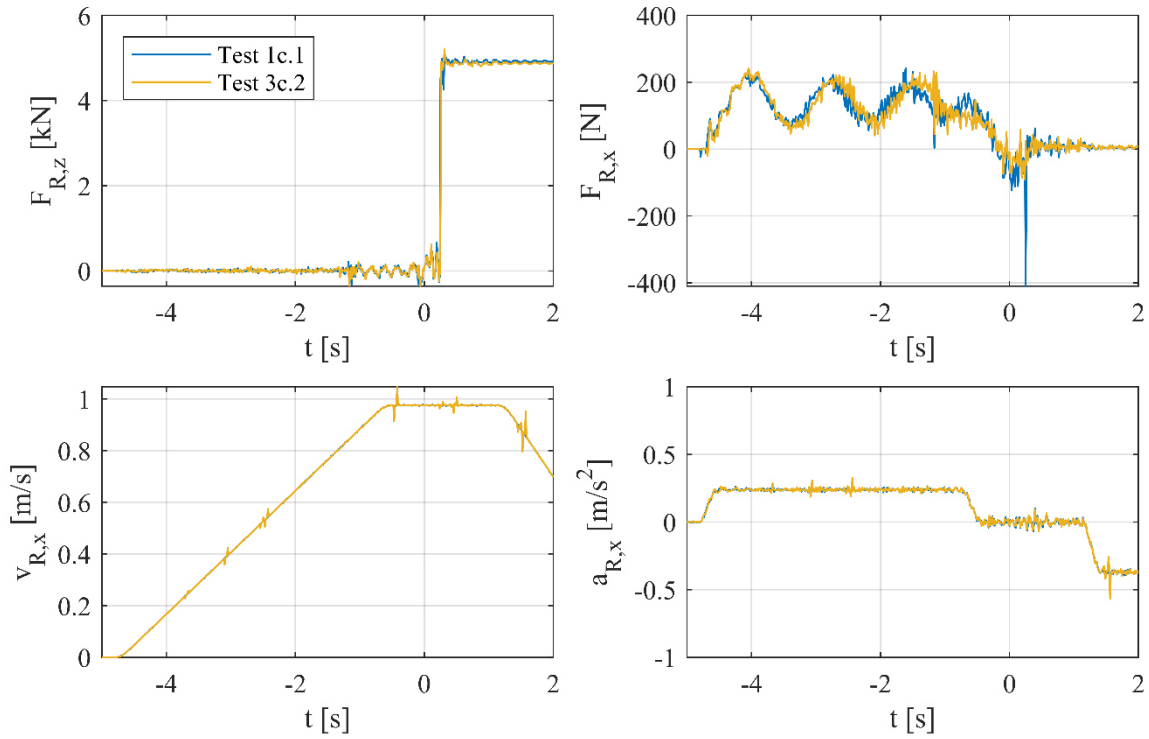

Figure 11: Robot interface forces and in vertical $F_{R,z}$ and flight direction $F_{R,x}$, robot velocities $v_{R,x}$ and accelerations $a_{R,x}$ for tests 1c.1 and 3c.2

Figure 12: Fluid behaviour before and after touchdown during test 3c.1

4.2. Landing behaviour

4.2.1. Landing Stability

In the following exemplary extractions of the stability analysis and fluid structure interaction analysis are given. Since this paper focuses on the test method, only examples are given and a more detailed analysis is found in [18].
In Figure 13 the landing sequence of the TDD is given. The TDD approaches its landing spot with a specific vertical and horizontal velocity (1). Right after touchdown (2), the horizontal landing velocity causes the TDD to tilt in flight direction until a maximum positive tilt angle is reached (3). If the tilt angle was greater than the stability threshold, the TDD would overturn. As in this campaign the stability threshold is not reached, the TDD is tilted back by gravity into its vertically neutral position. If the kinetic energy has not yet ceased, the TDD will tilt further until a maximum

DOI: 10.13009/EUCASS2025-214

negative tilt angle is reached (4), before tilting into flight direction again. This movement continues until the kinetic energy of the TDD has ceased.

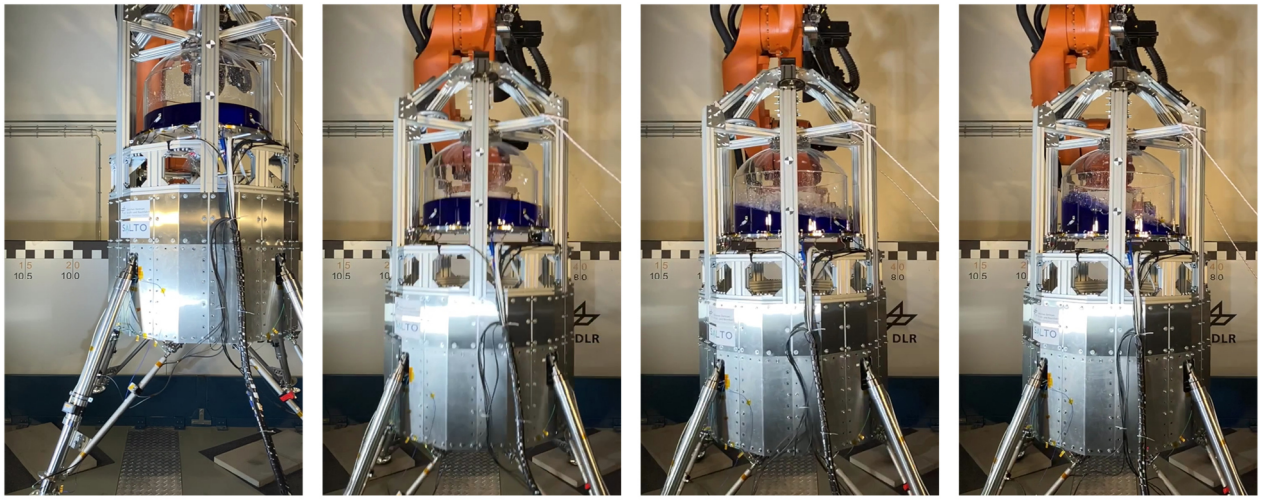

(1) -1.06 s (2) 0 s (3) 0.276 s (4) 0.678 s

Figure 13: Landing sequence of the TDD

The normalised tilt angles α_{norm}, which are the angular displacements in relation to the end position for test cases 1b, 2b and 3b are illustrated in Figure 14. It can be seen that the maximum α_{norm}, which are reached when the TDD is firstly tilted into flight direction, are approx. the same for all shown test cases. Also, the minimum α_{norm}, which are reached during the first tilt back, are similar. After this, the α_{norm} maxima and the total tilting amplitude decrease with increasing fluid mass, while the α_{norm} minima are lower for higher fluid levels. This implies smaller angular displacements when tilting in flight direction and larger angular displacements when tilting backwards for higher fluid levels. Further, the tilting motion decays faster with larger fluid masses. From this it can be concluded that the fluid causes a dampening effect on the TDD's tilting motion and thus improving landing stability.

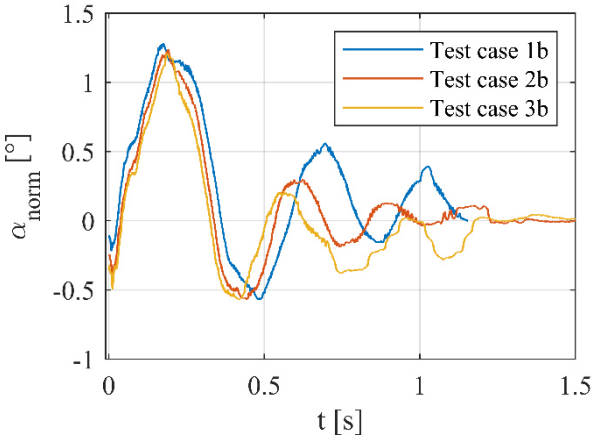

Figure 14: Normalised tilt angles α_{norm} for test cases 1b, 2b and 3b

4.2.2. Fluid Structure Interaction

Fluid-Structure interaction can be investigated at two positions, at the tank lander interfaces and at the tank baseplate. The measured forces in vertical direction at the tank lander interfaces $F_{tot,TL,v}$ are summed up and shown for test cases 1a, 2a and 3a in the left plot of Figure 15. The force response is characterised in the time domain by a compressive force peak at first ground contact and a following decaying low frequency oscillation, which is superimposed by a harmonic of higher frequency. It can be seen that with higher fluid levels and thus higher tank mass, the magnitude of the compressive force peak increases. Also, the amplitude of the harmonic increases with increasing fluid level and tank mass. For further investigation of the oscillation an amplitude spectrum of the total vertical tank force is analysed and shown in the right plot of Figure 15. Both the low frequency oscillation and the harmonic are clearly recognisable in the spectrum. For all three test cases the oscillation has a frequency of approximately 5.5 Hz. With increasing fluid

DOI: 10.13009/EUCASS2025-214

level, the fraction of this frequency in the overall signal increases. The harmonic is found at 40 Hz for test case 2a and at 35 Hz for test case 3a, respectively.

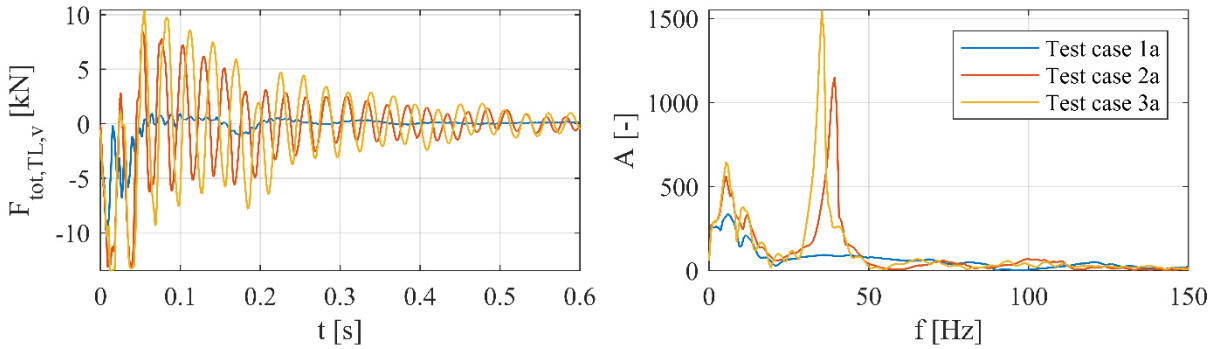

Figure 15: Total tank-lander interface forces in vertical direction $F_{tot,TL,v}$ and corresponding Amplitude spectrum for test cases 1a, 2a and 3a

For further investigation of the fluid impact on the structural responses of the tank base plate, shock response spectra of $Acc_{TBP,v}$ are analysed. In Figure 16 the logarithmic shock response spectra of the acceleration shocks at the tank baseplate for test cases 1a, 2a and 3a are given. These show that, in comparison to an empty tank, the presence of fluid in the tank causes an amplification at frequencies up to approx. 60 Hz, with the highest excitations at approx. 42 Hz. With higher fluid masses the amplification maximum decreases to 40 Hz. For frequencies higher than approx. 60 Hz, the fluid has a dampening effect, which intensifies with increasing fluid mass.

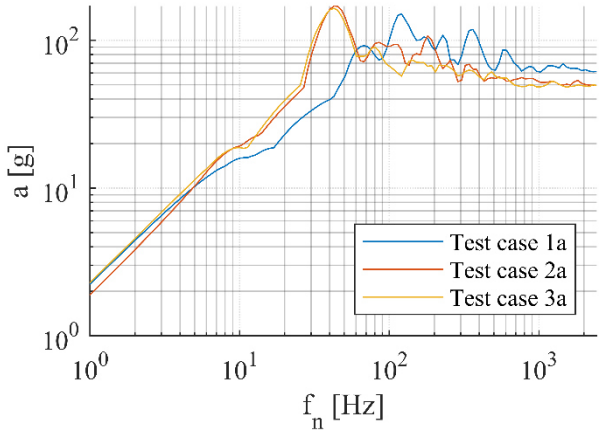

Figure 16: Shock response spectrum of Acceleration shocks at tank base plate for test cases 1a, 2a and 3a

5. Summary and Conclusion

Reusable launch vehicles that carry non-neglectable amount of fluid at the moment of touchdown face load cases that are new to the launcher domain. The sloshing fluid impacts landing behaviour and interacts with the launcher structure upon touchdown. Therefore, analyses of these interactions are indispensable for RLV design. Experimental investigations are necessary to gain first insights on the fluid sloshing impact at touchdown and to validate numerical models for further studies. This paper presents the experimental setup and execution of a test campaign to investigate the sloshing impact on fluid-structure interaction of vertically landing vehicles. The test object, a fully functional touchdown demonstrator and the used measurement system are presented in detail. Test results show that with the here presented setup repeatable landing conditions and repeatable landing behaviour can be achieved. Brief examples of the landing stability analysis and fluid-structure interaction analysis are given. From the stability analysis results that for this campaign the fluid has a stabilising effect on the vehicle motions during touchdown and the motions are damped by the fluid. Fluid structure interactions are examined at the tank-lander interfaces, where it is shown, that the vertical tank lander interface forces are characterised in the time domain by a compressive force peak at first ground contact and a following decaying low frequency oscillation, which is superimposed by a harmonic of higher frequency. With increasing fluid mass, the frequency of the harmonic decreases. Analyses of shock responds spectra of the acceleration shocks at the tank base plate reveal that in comparison to an empty tank, the presence of fluid in the tank causes an amplification at frequencies below approx. 60 Hz. Based on the test data obtained from this study, a flexible numerical

DOI: 10.13009/EUCASS2025-214

simulation model can be set up and validated and used for numerical parameter studies. This poses a time- and cost-efficient way to investigate the fluid impact for different vehicle parameters, varying tank configurations and fluids with different viscosities to determine stability boundaries, structural responses and interface forces for different touchdown scenarios.

DOI: 10.13009/EUCASS2025-214

References

[1] Doiron, H.H. and G. A. Zupp. 2000. Apollo Lunar Module Landing Dynamics. In 41st Structures, Structural Dynamics,and Materials Conference and Exhibit. American Institute of Aeronautics and Astronautics. Atlanta. GA

[2] Yu, Q., T. Wang, Z. Li. 2019. Rapid simulation of 3D liquid sloshing in the Lunar Soft-Landing spacecraft. AIAA Journal Vol 57

[3] Himeno, T. and T. Watanabe. 2005. Sloshing Prediction in the Propellant Tanks of VTVL Rocket Vehicle. 41st Joint Propulsion Conference & Exhibit, American Institute of Aeronautics and Astronautics, Tucson

[4] Himeno, T. et al. 2007. Numerical and Experimental Investigation on Sloshing in Rocket Tanks with Damping Devices, 43rd Joint Propulsion Conference & Exhibit, American Institute of Aeronautics and Astronautics, Cincinnati, OH

[5] Lance, A. 1966. Analysis of Propellant Slosh Dynamics and Generation of an Equivalent Mechanical Model For the Use in Preliminary Voyager Autopilot Design Studies, Technical Memorandum No. 33-306, Jet Propulsion Laboratory, California Institute of Technology

[6] Farì, S., D. Seelbinder, S. Theil. 2023. Advanced GNC-oriented modeling and simulation of Vertical Landing vehicles with fuel slosh dynamics. Acta Astronautica, 204

[7] Lunghi, P., P. Masarati, M. Lavagna. 2016. Multibody Modeling of Sloshing in Spacecraft Ascent and Landing Maneuvers, Proceedings of the ASME 2016 International Design Engineering Technical Conferences and Computers and Information in Engineering Conference, Vol. 6 Charlotte, NC

[8] Pei, J. 2021. Analytical Investigation of Propellant Slosh Stability Boundary on a Space Vehicle, Journal of Spacecraft and Rockets Vol. 58

[9] Nichkawde, C., P. M. Harish, N. Ananthkrishnan. 2004. Stability analysis of a multibody system model for coupled slosh–vehicle dynamics, Journal of Sound and Vibration

[10] Zhou, R. et al. 2012. Experimental and Numerical Investigation of Liquid Slosh Behavior Using Ground-Based Platforms. Journal of Spacecraft and Rockets Vol.49

[11] Meng, Y. et al. 2025. Predefined-Time Enhanced Antidisturbance Attitude Control for Rigid–Liquid Coupled Launch Vehicles, Journal of Guidance, Control and Dynamics

[12] Zhou, S., et al. 2023. Numerical simulation of sloshing in the propellant tank of reusable rocket vehicle using meshfree method, Computational Particle

[13] Guo, P. et al. 2024. Liquid propellant sloshing characteristics and suppression in new-generation space vehicle, Aerospace Systems

[14] Zwieten, T. et al. 2020. Nonlinear Slosh Damping Testing and Analysis for Launch Vehicle Propellant Tanks, AIAA Scitech 2020 Forum

[15] Anii, K. et al. 2019. Dynamics of Low-Gravity Sloshing in Spherical Tanks during Touchdown Phases of Landers, Proceedings of the AIAA Propulsion and Energy Forum

[16] Furuich, Y. et al. 2022. Evaluation of Sloshing Effect on a Tank during Landing Phases of Spacecrafts in a Micro-Gravity Environment, Proceedings of the AIAA Ascend Forum

[17] Roithmayr, C. M. and J. Pei. 2024. Effects of Propellant Slosh on Touchdown Stability for Landing Vehicles, Journal of Spacecraft and Rockets Vol 61

[18] Krämer, C. and L. Witte. 2024. Experimental Investigations of Fluid-to-Vehicle Interactions during a Reusable Launcher's Touchdown Impact. Pre-print CEAS Space Journal. https://doi.org/10.21203/rs.3.rs-4977412/v1

[19] Buchwald, R. et al. 2011. Verification of Landing System Touchdown Dynamics – A Status Report of a German Joint Cooperative Team on Landing Technology. Proceedings of the 62nd International Astronautical Congress, IAC-11.A3.1.3, Cape Town

[20] Krammer, A., L. Blecha, M. Lichtenberger. 2022. Fin actuation, thrust vector control and landing leg mechanisms design for the RETALT VTVL launcher. CEAS Space Journal 14

[21] Dumont, E. et al. 2021. CALLISTO: A Demonstrator for Reusable Launcher Key Technologies, Trans. JSASS Aerospace Tech. Japan Vol. 19

[22] https://www.dlr.de/de/forschung-und-transfer/forschungsinfrastruktur/grossforschungsanlagen/lande-und-mobilitaetsanlage. Accessed 04.08.2021

[23] Wilken, J. and S. Stappert. 2024. Comparative analysis of European vertical landing reusable first stage concepts, CEAS Space Journal

DOI: 10.13009/EUCASS2025-214

[24] Huang, M. 2019. Control strategy of launch vehicle and lander with adaptive landing gear for sloped landing, Acta Astronautica 161

[25] Benson, D. J. and P. A. Mason. 2011. Method for CFD Simulation of Propellant Slosh in a Spherical Tank. 47th AIAA/ASME/SAE/ASEE Joint Propulsion Conference and Exhibit

[26] Marwege, A. et al. 2019. Retro Propulsion Assisted Landing Technologies (RETALT): Current Status and Outlook of the EU Funded Project on Reusable Launch Vehicles, 70th International Astronautical Congress, Washington D.C.